Geophysical Research Letters®

Key Points:

- An extreme heat wave occurred in western North America (WNA) in the early summer of 2021, causing huge socioeconomic losses in several big cities
- The subseasonal activity of East Asian summer monsoon contributed to the occurrence of the heat wave via excitation of a Rossby wave train
- The East Asia-North America teleconnection can provide precursor signals for forecasting heat waves in WNA

Effects of Subseasonal Variation in the East Asian Monsoon System on the Summertime Heat Wave in Western North America in 2021

Yitian Qian[1] , Pang-Chi Hsu[1] , Jiacan Yuan[2] , Zhiwei Zhu[1] , Huijun Wang[1], and Mingkeng Duan[1]

[1]Key Laboratory of Meteorological Disaster, Ministry of Education, Nanjing University of Information Science & Technology, Nanjing, China, [2]Department of Atmospheric and Oceanic Sciences & Institute of Atmospheric Sciences, Fudan University, Shanghai, China

Abstract In the early summer (late June–early July) of 2021, a prolonged and extremely high temperature event was observed in the Northwest United States and Southwest Canada. In this study, a connection was found between the subseasonal variations of the East Asian monsoon system and the anomalous heat dome over western North America (WNA). Around 2–3 pentads prior to the period of maximum heat, a northward-propagating rain belt and abnormally intensified jet stream in East Asia excited a Rossby wave train, causing the high-pressure anomaly over WNA that was responsible for the occurrence of this heat wave in 2021. Multivariate singular value decomposition analysis results using historical data and a series of numerical experiments further supported the finding of this East Asia–western North America teleconnection. The results provide precursor signals for better monitoring and predicting heat waves over WNA.

Plain Language Summary A persistent and extremely high temperature event was observed in several states in the Northwest United States and Southwest Canada in summer 2021. This severe heat wave resulted in the hottest early-summer season in western North America (WNA) since 1979 and huge social and economic losses. Although the heat dome (high-pressure anomaly) over WNA was the factor responsible for this mega heat wave, the cause of this high-pressure anomaly was unclear. The present study reveals the importance of an atmospheric wave train emanating from East Asia toward North America in inducing the heat dome over WNA. The generation of the wave train is attributable to a northward-propagating rain belt and abnormally enhanced jet stream over East Asia from 10 to 15 days before the peak of this heat wave. Thus, monitoring the East Asian summer monsoon and associated wave train activity may help in predicting heat waves in WNA, and therefore in knowing when to put measures in place to mitigate against their effects.

1. Introduction

A record-breaking heat wave struck western North America (WNA) from late June through early July in 2021, which affected several large cities that otherwise rarely experience extreme heat waves, such as Portland, Oregon, and Seattle, Washington in the United States, and Vancouver in Canada. An extreme maximum temperature of 49.6°C—the highest ever recorded in Canada—was measured on 29 June in the village of Lytton (Schiermeier, 2021). There were more than 700 deaths—the majority believed to have been linked to the extreme heat (Murphy, 2021)—and 180 wildfires in the British Columbia, Canada (Schiermeier, 2021).

According to the observed daily surface air maximum temperature (T_{max}) data from the U.S. Climate Prediction Center (CPC/NOAA, 2021), extreme heat at 8°C higher than the climatological mean occurred over southwestern North America during 16–20 June 2021 (Figure 1a). Then, the high-temperature center moved toward northwestern North America, with the T_{max} reaching 41.3°C (about +16°C relative to the climatology) in the Canadian provinces of British Columbia and Alberta during 26–30 June (Figure 1c). In early July, although the heat wave weakened slightly over WNA (blue boxes), the T_{max} there still exceeded the 90th percentile (white cross-hatched areas in Figures 1d–1f). The area-averaged T_{max} over WNA showed "heat spike" days in early June, followed by exceptionally hot days during late June (Figure 1g). The peak temperature of 35.3°C was recorded on 28 June, which was far above the climatology (+13.1°C). The heat wave then dissipated around mid-July. Similar results were also observed in the ERA5 reanalysis data (not shown). This heat wave in WNA in 2021 (Figure 1) led to
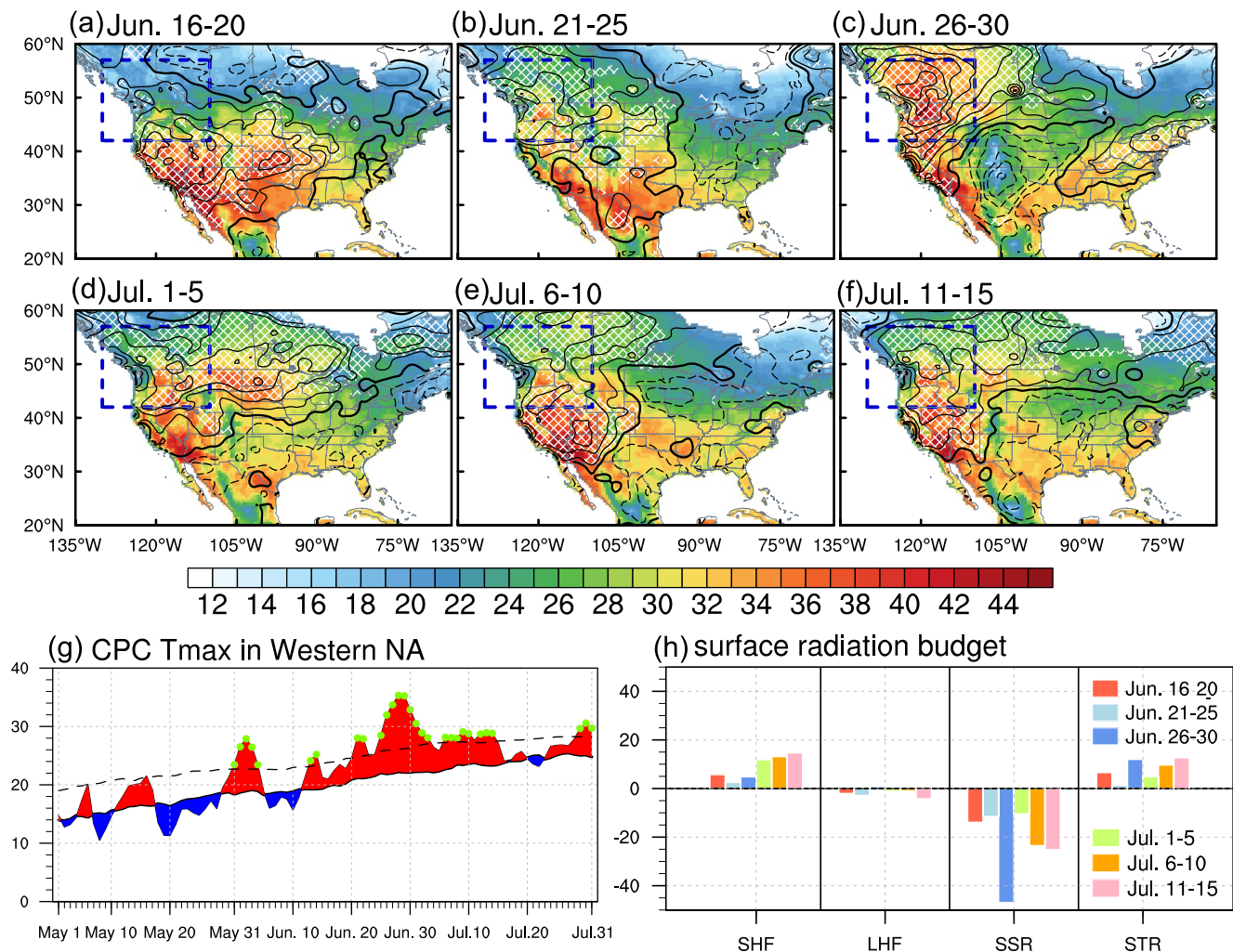
Figure 1. Temperature evolution in the early summer of 2021 over the North America. (a–f) Pentad-mean T_{max} (shading; units: °C) and its anomalies (contours with intervals of 2°C; dashed/solid contours for negative/positive anomalies) during 16 June–15 July 2021 derived from the Climate Prediction Center (CPC) data set. White hatching denotes those regions with T_{max} exceeding the 90th percentile. (g) Temporal evolution of the climatological (black curve) and anomalous (shading) T_{max} averaged over WNA (110°–140°W and 42°–57°N; blue boxes in upper panels) during May–July 2021. The dashed curve indicates the 90th percentile of T_{max} for each calendar day. Green dots label the dates with T_{max} exceeding the 90th percentile. (h) Surface energy budget terms over WNA in each pentad from mid-June to mid-July 2021 (units: W m^{-2}).

the hottest early-summer season over the past 40+ years (1979–2021) in the U.S. states of Oregon and Idaho, and the Canadian provinces of British Columbia and Alberta (Figure S1 in Supporting Information S1).

Scientists have reported that this heat wave in WNA in summer 2021 is unlikely to have happened without anthropogenic climate change, which increases the likelihood of such a heat wave occurring by at least 150 times relative to the conditions without human-induced climate change (Borenstein, 2021; Philip et al., 2021). In addition to the effect of global warming, blocking events and high-pressure anomalies associated with Rossby wave trains (RWTs) are commonly linked with the heat waves (Hsu et al., 2020; Lau & Kim, 2012, 2004; Luo & Lau, 2020; Schubert et al., 2011, 2014; Teng et al., 2013). RWTs are generally excited by atmospheric heating anomalies, which could be linked with precipitation, sea-surface temperature (SST) and land condition anomalies at various locations (Hu et al., 2019; Jong et al., 2020; Zhu & Li, 2016). In terms of this 2021 heat wave in WNA, a high-pressure anomaly hovered over the region persistently, like a lid on a pot trapping the heat within. The formation mechanisms of this "heat dome" (high-pressure anomaly) have not been fully clarified. Some researchers have attributed this extreme heat wave to the La Niña condition at that time and its associated circulation anomalies of the Pacific–North America (PNA) pattern (Gibbens, 2021; Thomas, 2021). However, the Niño3.4

index of −0.23°C during June–July 2021 indicated a weak La Niña state; it remains unclear whether this weak La Niña case is responsible for triggering the heat dome over WNA.

Recent studies have identified the East Asia-North America teleconnection, which modulates extreme events in various locations of North America during boreal summer (Lopez et al., 2019; Wang et al., 2001; Zhang et al., 2020; Zhu & Li, 2016). This motivated us to probe the possible effects of the East Asian summer monsoon (EASM) on the heat wave in WNA in summer 2021. The questions we sought to address were as follows: (a) Were there any abnormal and significant signals in the EASM system, such as the rain belt or jet stream, preceding and during the occurrence of the heat wave? and (b) How did the East Asia-North America teleconnection establish and influence this heat wave?

The rest of the paper is organized as follows: The data and methods are described in Section 2. Then, a possible formation mechanism for the heat dome involving teleconnection between the evolution of the EASM and surface air temperature anomalies in North America is proposed and further verified based on the results of a series of sensitivity experiments with an anomaly atmospheric general circulation model (AGCM) in Section 3. Conclusions are given in Section 4.

2. Data and Methods

2.1. Observational and Reanalysis Data

Observed daily T_{max} data were collected from the Climate Prediction Center (CPC) global temperature data set with a horizontal resolution of 0.5° × 0.5°. The Precipitation Estimation from the Remotely Sensed Information using Artificial Neural Networks-Climate Data Record (PERSIANN-CDR) data set provides high-resolution (0.25° × 0.25°) daily precipitation over the tropical to mid-latitude regions from 1983 to 2020 (Ashouri et al., 2015). To identify the deep convection activity, daily outgoing longwave radiation (OLR) data at a horizontal resolution of 2.5° × 2.5° from the polar-orbiting satellites of the National Oceanic and Atmospheric Administration (NOAA) (Liebmann & Smith, 1996) were employed.

To analyze the large-scale fields associated with this extreme heat event and diagnose the underlying mechanisms, daily zonal and meridional wind (u and v), vertical p-velocity (ω), temperature (T), and geopotential height (Z) at 21 vertical levels from 1000 to 100 hPa as well as surface variables including surface pressure (P_s), surface net shortwave radiation (SSR), surface net thermal radiation (STR), sensible heat flux (SHF) and latent heat flux (LHF), from the state-of-the-art ECMWF reanalysis data set, ERA5 (Hersbach et al., 2020), were utilized. The daily T_{max} data from ERA5 were also used, along with the observational data from CPC, to obtain robust results related to the heat wave.

According to the spatiotemporal evolution of the temperature anomaly over North America (Figures 1a–1g), the occurrence period of the heat wave was defined as 16 June–15 July 2021, which is consistent with most media reports. Heat wave days were identified as when the daily T_{max} exceeded the 90th percentile of the climatology. Considering the annual cycle of local temperature, we define the threshold for each calendar day with a 15-day window. For example, the 90th percentile value on 1 June was determined by the data from 25 May to 7 June during 1979–2020 (15days × 42 years = 630 samples).

2.2. Methods

2.2.1. Temperature and Surface Energy Budget Equations

To reveal the physical processes leading to this heat wave, the temperature budget equation was diagnosed. As shown in Equation 1, changes in temperature perturbations at each pressure level are contributed by the horizontal temperature advection, adiabatic process associated with vertical motion and static stability, and diabatic heating including small-scale physical processes:

$$\frac{\partial T'}{\partial t} = -(\mathbf{V} \cdot \nabla T)' + (\omega\sigma)' + \frac{Q'}{C_p} \tag{1}$$

in which prime indicates the perturbation components relative to the climatological summer (June–July) mean of 1979–2020, t is time in seconds, $\mathbf{V}$ is the horizontal velocity vector, ∇ is the horizontal gradient operator, and σ is the static stability, calculated as

$$\sigma = \frac{\partial T}{\partial P} - \frac{RT}{C_p P}. \tag{2}$$

Here, R is the gas constant, P is the pressure in Pa, and C_p is the specific heat at constant pressure.

The apparent heat source (Q) near the surface could be connected to the surface energy budget processes. As shown in Equation 3, the net upward heat flux through the surface (Fs) is determined by surface SSR, STR, SHF and LHF:

$$\text{Fs} = \text{SSR} + \text{STR} + \text{SHF} + \text{LHF} + G, \tag{3}$$

where G is the ground heat flux and is negligible (Kustas et al., 1993; Santanello Jr. & Friedl, 2003). All the fluxes are positive upward.

2.2.2. Rossby Wave Source and Wave Activity Flux

To detect the Rossby wave source (RWS) that triggered the teleconnection related to the heat wave, the anomalous RWS (S') was diagnosed (Sardeshmukh & Hoskins, 1988):

$$S' = -\overline{\zeta}\nabla \cdot \mathbf{V}'_\chi - \mathbf{V}'_\chi \cdot \nabla\overline{\zeta} - \zeta\nabla \cdot \overline{\mathbf{V}}_\chi - \overline{\mathbf{V}}_\chi \nabla\zeta', \tag{4}$$

where an overbar represents the climatological seasonal mean during June–July of 1979–2020, and a prime indicates the daily deviation from this climatological state. ζ is absolute vorticity. $\mathbf{V}_\chi$ is the divergent wind vector.

The anomalous horizontal wave activity flux (WAF) associated with a quasi-stationary RWT was proposed by Takaya and Nakamura (2001) as follows:

$$\mathbf{W} = \frac{p\cos\phi}{2|\mathbf{U}|}\left(\begin{array}{c} \dfrac{U}{a^2\cos\phi}\left[\left(\dfrac{\partial\psi'}{\partial\lambda}\right)^2 - \psi'\dfrac{\partial^2\psi'}{\partial\lambda^2}\right] + \dfrac{V}{a^2\cos\phi}\left[\dfrac{\partial\psi'}{\partial\lambda}\dfrac{\partial\psi'}{\partial\phi} - \psi'\dfrac{\partial^2\psi'}{\partial\lambda\partial\phi}\right] \\ \dfrac{U}{a^2\cos\phi}\left[\dfrac{\partial\psi'}{\partial\lambda}\dfrac{\partial\psi'}{\partial\phi} - \psi'\dfrac{\partial^2\psi'}{\partial\lambda\partial\phi}\right] + \dfrac{V}{a^2\cos\phi}\left[\left(\dfrac{\partial\psi'}{\partial\phi}\right)^2 - \psi'\dfrac{\partial^2\psi'}{\partial\phi^2}\right] \end{array}\right), \tag{5}$$

where $\mathbf{W}$ is the WAF; φ, λ and a represent the latitude, longitude and Earth's radius, respectively; $p =$ (pressure/1,000 hPa); $\mathbf{U} = (U, V)$ denotes climatological seasonal mean of the basic flow; and ψ' is the anomalous stream function.

2.2.3. Model Experiments

To confirm the contributions of the EASM on the heat wave, including the heating induced by the monsoon rain belt and the waveguide effect of the jet stream, a set of sensitivity experiments were conducted with the dynamic core of the Geophysical Fluid Dynamics Laboratory (GFDL) AGCM (Held & Suarez, 1994). This model is linearized by a three-dimensional climatological basic state to investigate responses to observed heating. The vertical coordinate of the model is five evenly distributed sigma levels ($=p/p_s$) with an interval of 0.2 started from a bottom level ($\sigma = 1$) to a top level ($\sigma = 0$), and the horizontal resolution is triangular 42 (T42). Realistic basic states including u, v, T, and P_s are derived from ERA5. More details about the primitive equations can be found in Supporting Information Text S1 in Supporting Information S1.

The model's capability in mimicking the effect of the preceding EASM anomalies on the heat wave in North America was first tested by prescribing the conditions during 16–20 June 2021 (2 pentads prior to the peak stage of the heat wave), including the mean states over the globe and the anomalous heating/cooling over East Asia, referred to as EXP_2021ANO. To reveal the relative effects of the precipitation-induced heating anomaly in the subtropical EASM region and the cooling anomaly in the Philippine Sea on the temperature changes in WNA, two experiments, EXP_2021HT and EXP_2021CL, were conducted by forcing either the heating or cooling alone, respectively. The basic states for EXP_2021HT and EXP_2021CL are prescribed the same with those in EXP_2021ANO. The essential role of the enhanced jet stream in the occurrence of this heat wave was verified

by another experiment, EXP_CLIMJET, in which the climatological pentad-mean (16–20 June) fields of u, v, T, P_s and the anomalous heating/cooling over East Asia during 16–20 June 2021 were used (against the results of EXP_2021ANO). The model was initialized with the forcing given by setting $t = 1$ day, and integrated for 60 days. The quasi steady state was approached after ~15 days.

3. Formation Mechanism of the Heat Wave

Figure 2 compares the spatiotemporal evolutions of the large-scale fields prior to and during the period of the heat wave. In the peak stage (26–30 June) of extreme heat, a suppressed convection anomaly (shading in the upper panel of Figure 2c) along with a quasi-barotropic high-pressure anomaly system at the levels of 500 and 200 hPa (the lower panel of Figure 2c) were evident over WNA. The temperature budget diagnostic results show the dominant contribution of adiabatic heating process during the developing stage of the WNA heat wave (Figure S2 in Supporting Information S1). In contrast, the anomalous horizontal temperature advection and diabatic heating effects were either negative or small. The subsidence of suppressed convection and the high-pressure anomaly induced a clear sky, enhancing the downward SSR to heat up the surface, and then the increased STR and SHF (Figure 1h) warmed the surface air.

The source of the local high-pressure anomaly (the "heat dome") could be linked to the RWT that was triggered by the convective heating near the East Asian jet stream (pink shading and blue dots near the red contours in the upper panel of Figure 2c) and emanated along the westerly jet toward North America (vectors in Figure 2c). This RWT initiated around mid-June (Figure 2a) and enhanced persistently (Figures 2b and 2c) when the high-level divergence associated with the EASM rain belt anomaly appeared over the subtropical western North Pacific (WNP) and moved northwards toward the jet stream (the area with large vorticity). Among the physical processes of RWS generation [S' in Equation 4], the stretching of climatological absolute vorticity by the anomalous divergent flow ($-\bar{\zeta}\nabla \cdot V'_\chi$) is the major contributor (Figure S3 in Supporting Information S1). Meanwhile, the jet stream intensified and extended eastwards abnormally (red contours in Figures 2b and 2c) compared to the pentad climatological state (light blue contours), providing a more efficient waveguide for teleconnection (Branstator, 1983; Teng et al., 2013; Zhang et al., 2020; Zhu & Li, 2016, 2018). The enhancement and eastward extension of the jet stream was related to the strengthening of the meridional temperature gradient when the suppressed convection anomaly induced a warm anomaly over the subtropical WNP (150°E−180° and 20°–40°N) (not shown). From early to mid-July (Figures 2d–2f), the monsoon rain belt and jet stream weakened, and the RWT became less organized. The heat dome over WNA gradually dissipated. Note that the pattern of the East Asia-North America teleconnection leading to the heat dome (Figure 2) is distinct from the typical PNA pattern associated with tropical Pacific SST anomalies (Horel & Wallace, 1981; Jong et al., 2020) suggesting that the weak La Niña event might have played a minor role in inducing this heat wave in summer 2021 simultaneously. However, how and to what extent the La Niña in the previous winter could exert a delayed impact on the following EASM and its teleconnection (Wang et al., 2001) are unsolved issues that require further study (Supporting Information Text S2 and Figure S4 in Supporting Information S1).

Although the East Asia-North America teleconnection was clearly apparent in the case of this heat wave in WNA in summer 2021 (Figure 2), long-term (1983–2020) historical data were further used to confirm whether this teleconnection pattern is a robust signal for triggering high temperature events in WNA more generally. To elucidate the joint effects of the EASM system (including precipitation and 200-hPa zonal wind over [100°E−180° and 10°–55°N]) on the T_{max} in North America (60°–135°W and 15°–65°N), a multivariate singular value decomposition (SVD) analysis was performed (Figure 3). Notably, the first leading mode, accounting for 20.8% of the explained covariance, identifies the association between anomalous EASM activity and high temperature conditions over WNA. A tripole pattern of T_{max} anomalies over North America (i.e., significant high temperature anomalies in northwestern and southern North America, but a low temperature anomaly in central-eastern North America) (Figure 3b) is closely coupled with the subtropical precipitation and enhanced jet stream over East Asia (Figure 3a).

To confirm the influences of EASM-associated anomalies on the WNA heat wave, the composites of the preceding large-scale precipitation and wind fields relative to the peak of high temperature over WNA are plotted. Day 0 is the day when the standardized expansion coefficient of the first leading SVD mode of the T_{max} anomaly over North America exceeds one standard deviation. Lead N days indicate the large-scale fields in N days before Day 0. From 8 to 14 days before the peak of high temperature over WNA (Figures 3c–3f), the EASM rainfall appears
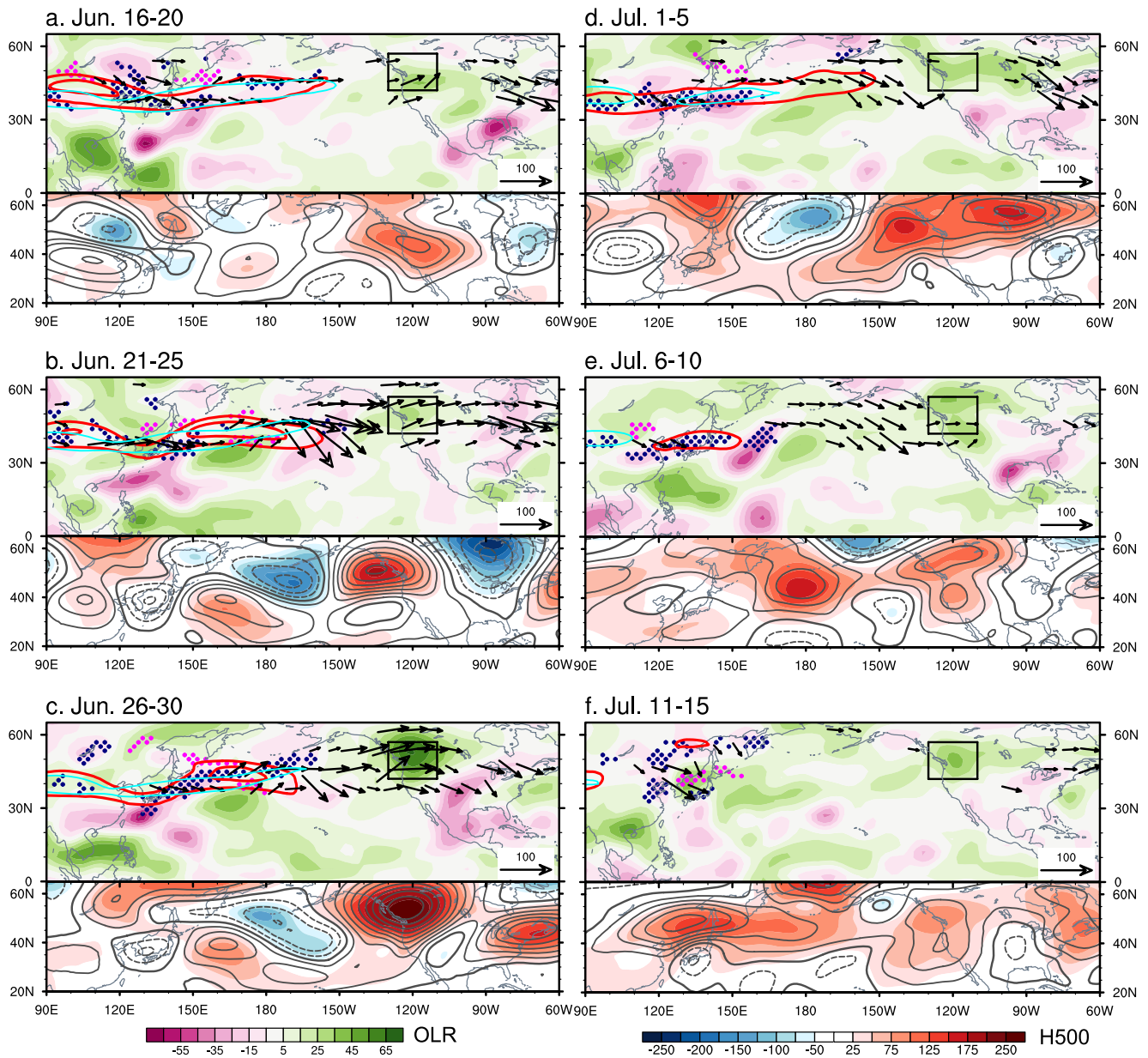
Figure 2. Evolutions of large-scale fields associated with the western North America (WNA) heat wave. Pentad evolutions of the (upper panel of each sub-figure) observed outgoing longwave radiation (OLR) anomaly (shading; units: W m^{-2}), westerly jet represented by zonal wind (red contours; start from 30 m s^{-1} with an interval of 20 m s^{-1}), and anomalous Rossby wave source (values smaller [larger] than -5×10^{10} s^{-2} [5×10^{10} s^{-2}] are indicated by dark blue [pink] dots) and WAF (black vectors; units: m^2 s^{-2}) at 200 hPa, and the (lower panel of each sub-figure) geopotential height anomaly at 500 hPa (shading; units: gpm) and 200 hPa (gray contours with an interval of 30 gpm). (a–f) represent the results of 16–20 June, 21–25 June, 26–30 June, 1–5 July, 6–11 July, and 11–15 July in 2021, respectively. The climatological pentad-mean of the westerly jet (defined by 200-hPa zonal wind = 30 m s^{-1}) is shown by the light blue contours. The black box (110°–130°W and 42°–57°N) delineates the region of WNA.

over the subtropical region, and the 200-hPa zonal wind extends toward the central Pacific. The RWT is seen with relatively weak amplitude. Accompanied by the enhancement of EASM precipitation and jet stream, the RWT strengthens in the following periods, forming a positive high-pressure anomaly associated with heat waves in WNA (Figures 3g–3j). The evolution of the large-scale conditions associated with North American T_{max} derived from SVD1 (Figure 3) closely resemble the case in 2021 (Figure 2). The results signify a robust connection between North American heat events and EASM activity (Lopez et al., 2019; Yang et al., 2020).
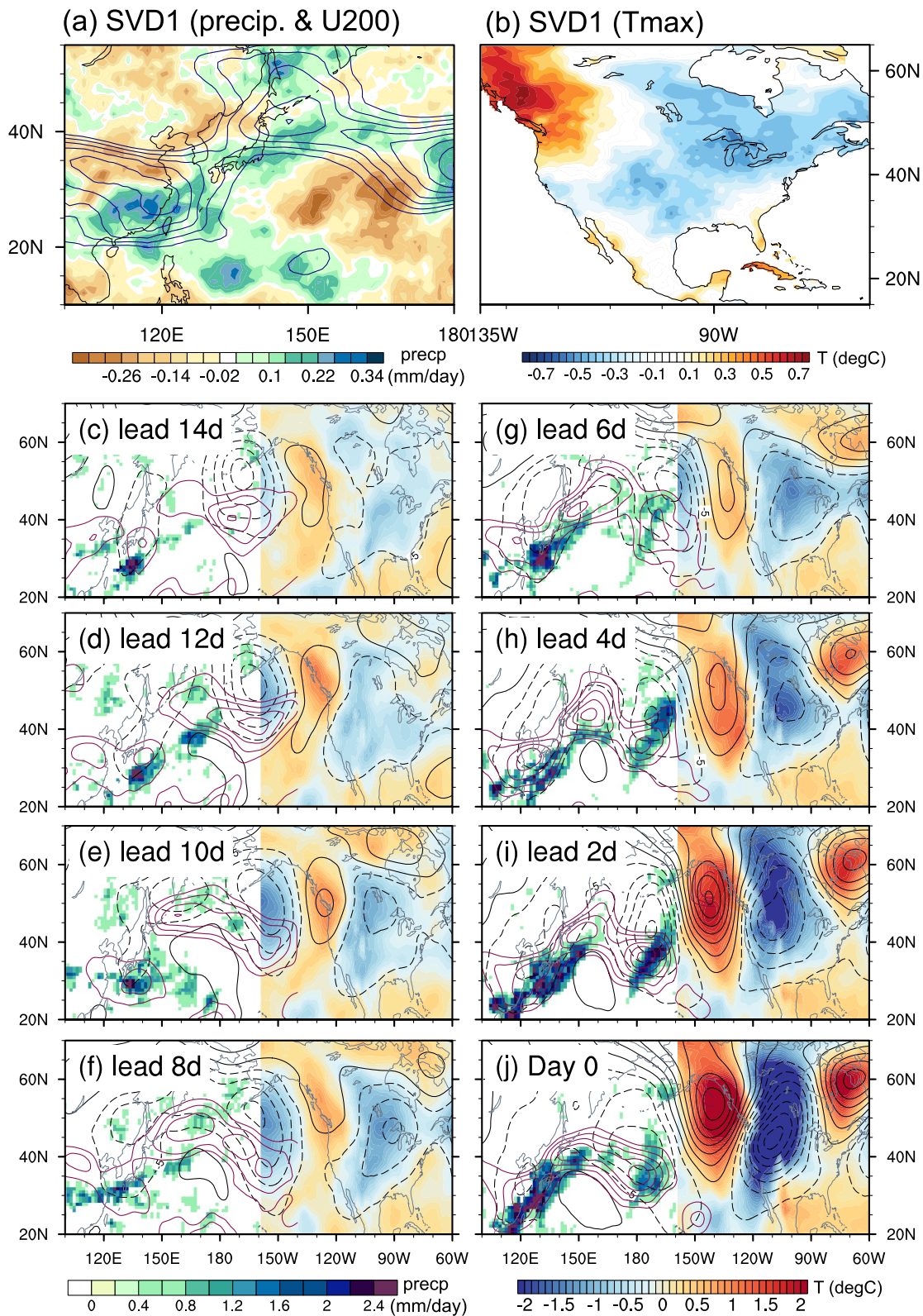
Figure 3.

The relative roles of monsoon rainfall-related heating anomalies and jet steam intensity in causing the heat wave in WNA were clarified by carrying out sensitivity experiments as described in Section 2.2.3. The results of EXP_2021ANO show the capability of the AGCM in simulating the large-scale RWT emanating from East Asia and inducing the high-pressure anomaly over WNA (left panel of Figure 4a) as observed (Figures 2 and 3). The high-pressure anomaly (middle panel of Figure 4a) and positive temperature anomaly (right panel of Figure 4a) in WNA both increase with integration time and reach their maximum around 10–15 days (Figures 2 and 3). The distinct effects of rain belt-induced heating in the subtropical WNP (left panel of Figure 4b) and cooling in the tropical western Pacific (left panel of Figure 4c) were examined by comparing the results of EXP_2021HT (Figure 4b) and EXP_2021CL (Figure 4c). The positive anomalies of geopotential height and temperature over WNA are only shown in the results of EXP_2021HT (Figure 2b). In contrast, an opposite phase of the RWT and decreased geopotential height and temperature over WNA appear in the results of EXP_2021CL (Figure 4c). This suggests that the subtropical rain belt-induced heating alone (without the cooling in the tropics) may have forced the RWT relevant to this heat wave in WNA. Note that the results remained the same if we only prescribed the background mean state in 2021 over the East Asia-WNP region (60°E−180°, 0°–90°N) but the climatological mean state elsewhere, implying that the high temperature anomaly over WNA was indeed related to remote forcing rather than local effects. The simulation produced by EXP_CLIMJET highlights the importance of the extremely enhanced jet stream in the early-summer of 2021 in causing the heat wave. Once the climatological 3-D wind fields were prescribed, the RWT was weakened and shifted westwards (left panel of Figure 4d), as compared to the 2021 case (left panel of Figure 4a). Very small changes in geopotential height and temperature were measured in WNA (middle and right panels of Figure 4d). Therefore, the enhancement and eastward extension of the jet stream (Figures 2a–2d) were essential for the occurrence of this heat wave in WNA. To enhance the robustness of the modeling results, we generated five ensemble members by forcing individually the daily heating/cooling anomalies from 16 to 20 June in individual experiments and conducted ensemble averages (Figure S5 in Supporting Information S1). The ensemble results are largely consistent with the current results (Figure 4).

4. Conclusions

A record-breaking heat wave in the early summer (16 June–15 July) of 2021, with temperatures 16°C higher than the climatology, affected WNA, including several states in the Northwest United States and Southwest Canada (Figure 1). In addition to the effect of human-induced climate change (Borenstein, 2021; Philip et al., 2021), this study has identified the important contribution of East Asia-North America teleconnection to the occurrence of the heat dome that triggered and maintained the local extreme heat condition over WNA.

The local high-pressure anomaly over the heat wave region was observed to be part of a RWT emanating from East Asia generated by the combined effect of the subseasonal rain belt and jet stream variations (Figure 2). With the monsoon rain belt appeared over the subtropical WNP and moved northwards toward the south of the East Asian jet stream, the precipitation-induced heating and background vorticity gradient associated with the jet stream excited the RWT in the upper troposphere. Then, the jet stream intensified and extended eastwards, serving as an efficient waveguide for the Rossby wave energy propagating toward North America, inducing a subsidence anomaly appeared to the south of the jet exit area. It warmed the temperature there and resulted the occurrence of the extreme heat wave in WNA.

The teleconnection between North American T_{max} and EASM activity at the subseasonal timescale could be clearly seen in multivariate SVD analysis results using long-term (1983–2020) daily data (Figure 3). Model experiments also supported the observational findings that the subtropical precipitation and intensified jet stream over East Asia played critical roles in the generation and maintenance of this heat wave in WNA through teleconnection (Figure 4).

The East Asia-North America teleconnection pattern has been documented in some recent studies (Lopez et al., 2019; Zhang et al., 2020; Zhu & Li, 2016) at monthly and seasonal time scales. The subseasonal changes in

Figure 3. Singular value decomposition (SVD) analysis and composited evolutions of precipitation and westerly jet in the East Asia and temperature in the North America. The first leading SVD mode of (a) (left) precipitation anomalies (shading) and 200-hPa zonal wind anomalies (blue contours) over East Asia (100°E−180°and 10°–55°N) and (b) (right) T_{max} anomalies (shading; units: °C) over North America (60°–135°W, 15°–65°N) during 16 June–15 July of 1983–2020. (c–j) Evolutions of the East Asian precipitation anomaly (shading to the west of 140°W), 850-hPa North American temperature anomaly (units: °C; shading to the east of 140°W), 200-hPa zonal wind anomalies (purple contours staring from 1 with an interval of 1 m s⁻¹), and 200-hPa geopotential height anomaly (units: gpm; contours with an interval of 10 gpm), composited for a lead time of (c) 14, (d) 12, (e) 10, (f) 8, (g) 6, (h), (i) 2 days, and (j) day 0.
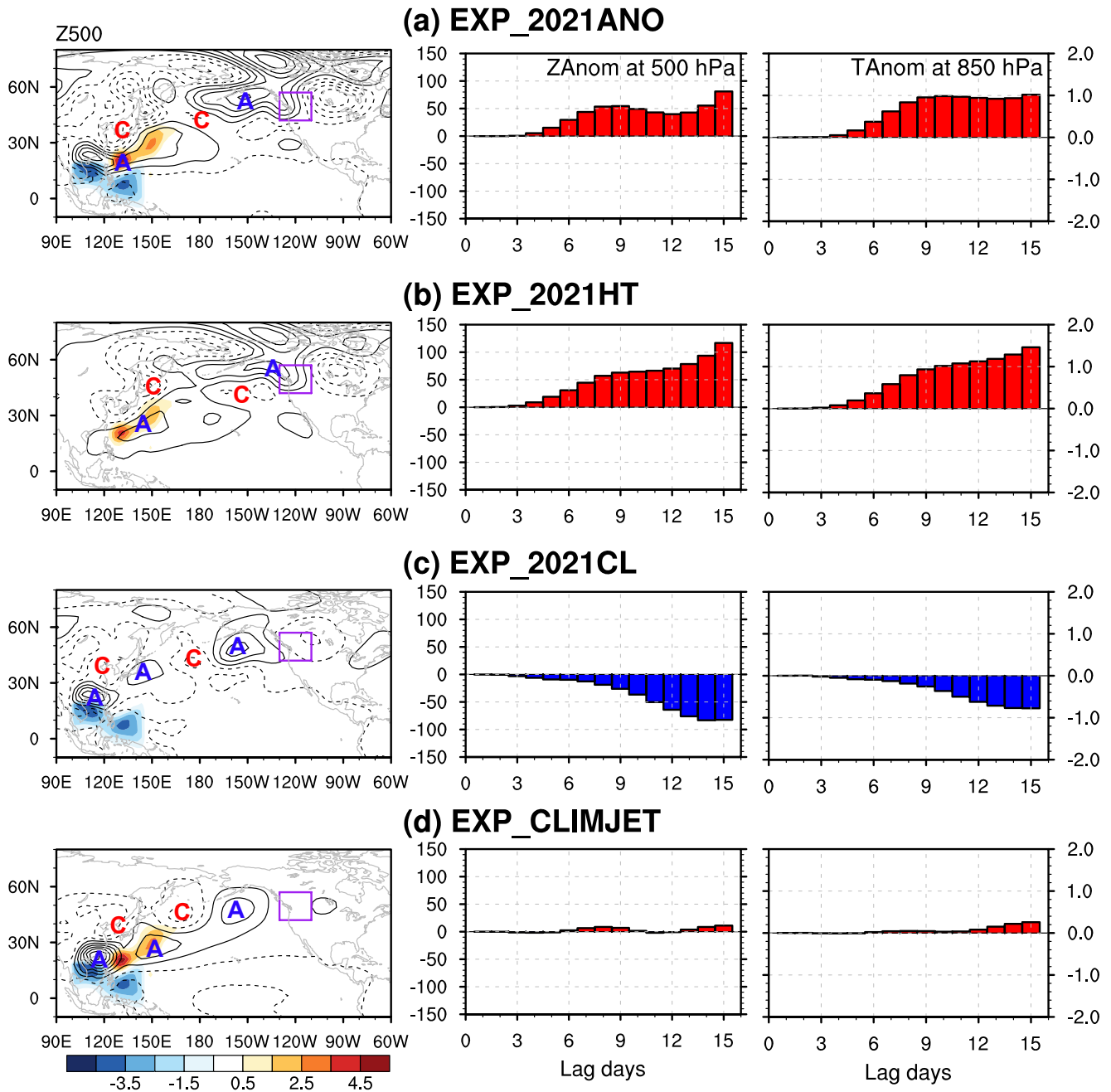
Figure 4. Sensitive experiments for verifying the crucial roles in western North America (WNA) heat wave occurrence. (left) Simulated 500-hPa geopotential height (contours; start from 25 gpm with an interval of 50 gpm; units: gpm) and heating anomaly (shading; units: K day^{-1}) integrated at day 10 in (a) EXP_2021ANO, (b) EXP_2021HT, (c) EXP_2021CL, and (d) EXP_CLIMJET experiments, respectively. (Middle and right) As in (left) but for the temporal evolution of the WNA (110°–140°W, 42°–57°N; purple boxes in the left panel) area-averaged 500-hPa geopotential height anomaly (units: gpm) and 850-hPa temperature anomaly (units: K). The letters "A" and "C" indicate the centers of anticyclonic and cyclonic anomalies, respectively.

the EASM rainfall and jet stream prior to and during the occurrence of heat waves provide valuable information for monitoring and forecasting such natural disasters over WNA. How the East Asia-North America teleconnection is predicted by operational models and whether this teleconnection can serve as a source of subseasonal predictability for North American heat waves are the two open issues that will be addressed in future work using the data sets of the Subseasonal-to-Seasonal Prediction Project (Vitart et al., 2017).

Data Availability Statement

The T_{max} data were obtained from the Climate Prediction Center (CPC) global daily temperature data set (https://www.psl.noaa.gov/data/gridded/data.cpc.globaltemp.html). The large-scale fields were based on ERA5 data (https://doi.org/10.24381/cds.bd0915c6). The daily precipitation data set was derived from PERSIANN-CDR (https://www.ncei.noaa.gov/data/precipitation-persiann/access/). The NOAA OLR data were from https://psl.noaa.gov/data/gridded/data.interp_OLR.html. The simulations of the AGCM sensitive experiments are available online (https://doi.org/10.5281/zenodo.6370953).

References

Ashouri, H., Hsu, K.-L., Sorooshian, S., Braithwaite, D., Knapp, K. R., & Cecil, L. D. (2015). Daily precipitation climate data record from multi-satellite observations for hydrological and climate studies. *Bulletin of the American Meteorological Society*, *94*, 69–83. https://doi.org/10.1175/bams-d-13-00068.1

Borenstein, S. (2021). *Northwest heat wave impossible without climate change*. Retrieved from https://apnews.com/article/climate-climate-change-science-environment-and-nature-935be069af34aad472074d42097af85e

Branstator, G. (1983). Horizontal energy propagation in a barotropic atmosphere with meridional and zonal structure. *Journal of the Atmospheric Sciences*, *40*(7), 1689–1708. https://doi.org/10.1175/1520-0469(1983)040<1689:hepiab>2.0.co;2

CPC/NOAA. (2021). Retrieved from https://www.psl.noaa.gov/data/gridded/data.cpc.globaltemp.html

Gibbens, S. (2021). https://www.nationalgeographic.com/environment/article/heat-dome-deadly-hot-weather-descends-on-pacific-northwest

Held, I. M., & Suarez, M. J. (1994). A proposal for the intercomparison of the dynamical cores of atmospheric general-circulation models. *Bulletin of the American Meteorological Society*, *75*, 1825–1830. https://doi.org/10.1175/1520-0477(1994)075<1825:apftio>2.0.co;2

Hersbach, H., Bell, B., Berrisford, P., Hirahara, S., Horányi, A., Muñoz-Sabater, J., et al. (2020). The ERA5 global reanalysis. *Quarterly Journal of the Royal Meteorological Society*, *146*, 1999–2049. https://doi.org/10.1002/qj.3803

Horel, J. D., & Wallace, J. M. (1981). Planetary-scale Atmospheric phenomena associated with the Southern Oscillation. *Monthly Weather Review*, *109*(4), 813–829. https://doi.org/10.1175/1520-0493(1981)109<0813:psapaw>2.0.co;2

Hsu, P.-C., Qian, Y., Liu, Y., Murakami, H., & Gao, Y. (2020). Role of abnormally enhanced MJO over the Western Pacific in the formation and subseasonal predictability of the record-breaking Northeast Asian heatwave in the summer of 2018. *Journal of Climate*, *33*, 3333–3349. https://doi.org/10.1175/JCLI-D-19-0337.1

Hu, W., Liu, P., Zhang, Q., & He, B. (2019). Dominant patterns of winter-time intraseasonal surface air temperature over the CONUS in response to MJO convections. *Climate Dynamics*, *53*, 3917–3936. https://doi.org/10.1007/s00382-019-04760-x

Jong, B., Ting, M., Seager, R., & Anderson, W. B. (2020). ENSO teleconnections and impacts on U.S. summertime temperature during a multi-year La Niña life cycle. *Journal of Climate*, *33*(14), 6009–6024. https://doi.org/10.1175/JCLI-D-19-0701.1

Kustas, W. P., Daughtry, C. S. T., & van Oevelen, P. J. (1993). Analytical treatment of the relationships between soil heat flux/net radiation ratio and vegetation indices. *Remote Sensing of Environment*, *46*, 319–330. https://doi.org/10.1016/0034-4257(93)90052-y

Lau, W. K. M., & Kim, K.-Y. (2012). The 2010 Pakistan flood and Russian heat wave: Teleconnection of hydrometeorological extremes. *Journal of Hydrometeorology*, *13*(1), 392–403. https://doi.org/10.1175/JHM-D-11-016.1

Liebmann, B., & Smith, C. A. (1996). Description of a complete (interpolated) outgoing longwave radiation dataset. *Bulletin of the American Meteorological Society*, *77*(6), 1275–1277.

Lopez, H., Lee, S.-K., Dong, S., Goni, G., Kirtman, B., Atlas, R., & Kumar, A. (2019). East Asian Monsoon as a modulator of U.S. Great Plains heat waves. *Journal of Geophysical Research: Atmospheres*, *124*, 6342–6358. https://doi.org/10.1029/2018JD030151

Luo, M., & Lau, N.-C. (2020). Summer heat extremes in northern continents linked to developing ENSO events. *Environmental Research Letters*, *15*(7), 074042. https://doi.org/10.1088/1748-9326/ab7d07

Murphy, J. (2021). BBC https://www.bbc.com/news/world-us-canada-58015089

Philip, S. Y., Kew, S. F., van Oldenborgh, G. J., Anslow, F. S., Seneviratne, S. I., Vautard, R., et al. (2021). Rapid attribution analysis of the extraordinary heatwave on the Pacific Coast of the US and Canada June 2021. *Earth System Dynamics*. https://doi.org/10.5194/esd-2021-90

Santanello, J. A., Jr., & Friedl, M. A. (2003). Diurnal covariation in soil heat flux and net radiation. *Journal of Applied Meteorology and Climatology*, *42*(6), 851–862. https://doi.org/10.1175/1520-0450(2003)042<0851:dcishf>2.0.co;2

Sardeshmukh, P. D., & Hoskins, B. J. (1988). The generation of global rotational flow by steady idealized tropical divergence. *Journal of the Atmospheric Sciences*, *45*(7), 1228–1251. https://doi.org/10.1175/1520-0469(1988)045<1228:tgogrf>2.0.co;2

Schiermeier, Q. (2021). Climate change made North America's deadly heatwave 150 times more likely. *Nature*. https://www.nature.com/articles/d41586-021-01869-0

Schubert, S. D., Suarez, M. J., Pegion, P. J., Koster, R. D., & Bacmeister, J. T. (2004). Causes of long-term drought in the U.S. Great plains. *Journal of Climate*, *17*(3), 485–503. https://doi.org/10.1175/1520-0442(2004)017<0485:coldit>2.0.co;2

Schubert, S. D., Wang, H., Koster, R. D., & Suarez, M. J. (2014). Northern Eurasian heat waves and droughts. *Journal of Climate*, *27*(9), 3169–3207. https://doi.org/10.1175/JCLI-D-13-00360.1

Schubert, S. D., Wang, H., & Suarez, M. J. (2011). Warm season subseasonal variability and climate extremes in the Northern Hemisphere: The role of stationary Rossby waves. *Journal of Climate*, *24*(18), 4773–4792. https://doi.org/10.1175/JCLI-D-10-05035.1

Takaya, K., & Nakamura, H. (2001). A formulation of a phase independent wave-activity flux for stationary and migratory quasi-geostrophic eddies on a zonally varying basic flow. *Journal of the Atmospheric Sciences*, *58*(6), 608–627. https://doi.org/10.1175/1520-0469(2001)058<0608:afoapi>2.0.co;2

Teng, H., Branstator, G., Wang, H., Meehl, G. A., & Washington, W. M. (2013). Probability of US heat waves affected by a subseasonal planetary wave pattern. *Nature Geoscience*, *6*, 1056–1061. https://doi.org/10.1038/NGEO1988

Thomas, E. (2021). https://www.actionnews5.com/2021/07/07/breakdown-heat-dome-why-northwest-experienced-historic-heat-wave/

Vitart, F., Ardilouze, C., Bonet, A., Brookshaw, A., Chen, M., Codorean, C., et al. (2017). The subseasonal to seasonal (S2S) prediction project database. *Bulletin of the American Meteorological Society*, *98*(1), 163–173. https://doi.org/10.1175/BAMS-D-16-0017.1

Wang, B., Wu, R., & Lau, K.-M. (2001). Interannual variability of the Asian summer monsoon: Contrasts between the Indian and the Western North Pacific–East Asian monsoons. *Journal of Climate*, *14*, 4073–4090. https://doi.org/10.1175/1520-0442(2001)014<4073:ivotas>2.0.co;2

Yang, Y., Zhu, Z., Li, T., & Yao, M. (2020). Effects of the Western Pacific intraseasonal convection on the surface air temperature anomalies over North America. *International Journal of Climatology*, *40*(6), 2913–2923. https://doi.org/10.1002/joc.6373

Zhang, W., Villarini, G., & Vecchi, G. A. (2020). The East Asian subtropical jet stream and Atlantic tropical cyclones. *Geophysical Research Letters*, *47*, e2020GL088851. https://doi.org/10.1029/2020GL088851

Zhu, Z., & Li, T. (2016). A new paradigm for continental U.S. summer rainfall variability: Asia-North America teleconnection. *Journal of Climate*, *29*(20), 7313–7327. https://doi.org/10.1175/JCLI-D-16-0137.1

Zhu, Z., & Li, T. (2018). Amplified contiguous United States summer rainfall variability induced by East Asian monsoon interdecadal change. *Climate Dynamics*, *50*(9–10), 3523–3536. https://doi.org/10.1007/s00382-017-3821-8

References From the Supporting Information

Lin, H. (2019). Long-lead ENSO control of the boreal summer intraseasonal oscillation in the East Asian-Western North Pacific region. *npj Climate and Atmospheric Science*, *2*, 31. https://doi.org/10.1038/s41612-019-0088-2

Ye, D., & Huang, R. (1996). *Study about mechanism of drought and flood around Changjiang river and Huanghe river* (p. 387). Shandong Science and Technique Press. (in Chinese).